Available online at www.sciencedirect.com
SCIENCE DIRECT®
Electrochimica Acta 49 (2004) 657–665
ELECTROCHIMICA Acta
www.elsevier.com/locate/electacta

The study of the proton diffusion process in the porous MnO_2 electrode

Deyang Qu*

Emtech, 2486 Dunwin Dr., Mississauga, Ont., Canada

Received 10 May 2003; received in revised form 28 July 2003; accepted 21 August 2003

Abstract

The proton diffusion coefficients in an electrolytic manganese dioxide (EMD) electrode at various stages of the constant current discharge have been determined by means of AC impedance technique. The finite diffusion model was applied in the numerical fitting. The crystallite size of EMD was estimated from (1 1 0), (1 2 1) and (0 2 1) diffraction peaks with both Scherrer equation and Warren–Averbach theory. X-ray diffraction (XRD) peak broadening caused by instrument, crystallite size and microstrain was separated. The crystallite size of ramsdellite was assumed to be the proton diffusion length.

Keywords: MnO_2; Proton diffusion coefficient; AC impedance; Crystallite size; Finite diffusion model

1. Introduction

MnO_2 has been used as cathode material in many battery systems for decades, for example, electrolytic manganese dioxide (EMD) in primary/secondary alkaline batteries and spinel Lithium manganese dioxide in rechargeable Li-ion cells. MnO_2 has also been proved as one of the most inexpensive, abundant and non-toxic cathodic battery reactants with very good performance. The mechanism of the MnO_2 discharge in alkaline KOH solution has been extensively studied for some decades. Among such mechanisms, the scheme of Kozawa and co-workers [1–4] seems to be widely adopted, in which a two-step mechanism was postulated for γ-MnO_2 to $Mn(OH)_2$. Conversion of MnO_2 to $MnO_{1.5}$ is the first step, in which the crystal structure of γ-MnO_2 is preserved. After H_2O molecules become decomposed on the surface of MnO_2, protons diffuse within MnO_2 through the tunnels inside the structure. The step is homogeneous, thus a slope discharge curve is demonstrated. The second step involves further reduction of $MnO_{1.5}$ to $Mn(OH)_2$, since most of the vacancies inside the lattice of MnO_2 are occupied by protons, the second step of the reduction is a heterogeneous surface reaction involving soluble intermediate Mn(III) species. The "so-called" γ-structure of the material starts to collapse at the beginning of the second reduction step. Practically, EMD is hardly discharged beyond the first electron in alkaline cells, thus it is critical to understand the behavior of the proton diffusion process inside the lattice of MnO_2, the process was suggested as a slow and rate determine step during the reduction of MnO_2 [6].

The proton diffusion within MnO_2 has been studies by means of various electrochemical techniques, since being advanced by Coleman [7]. Scott [8] proposed a simple model for the measurement of proton diffusion coefficient (D_H) inside MnO_2 based on the semi-infinite diffusion model. In 1962, Kornfeil [9], also based on the semi-infinite diffusion model, calculated the proton diffusion coefficient by means of fitting the potential recovery curves of the MnO_2 electrode. Atlung and Jacobsen [5] investigated the proton diffusion process of EMD in potassium chloride/potassium hydroxide electrolyte by AC impedance technique. Chabre and Pannetier [6] measured the proton diffusion coefficient of EMD at various stages of the discharge by SPEC.

Almost all the published works on the studies of the proton diffusion inside the lattice of MnO_2 have been based on the assumption of the semi-infinite diffusion. In order to estimate the proton diffusion coefficient using the semi-infinite diffusion model, the electrochemically accessible surface area and the molar volume of MnO_2 at various stages of the discharge need to be determined. The difficulties of estimating

* Present address: Rayovac Corporation, 601 Rayovac Dr., Madison, WI 53711, USA. Tel.: +1-608-275-4745; fax: +1-608-275-4992.
E-mail address: qu@rayovac.com (D. Qu).

0013-4686/$ – see front matter © 2003 Elsevier Ltd. All rights reserved.
doi:10.1016/j.electacta.2003.08.030

the accessible surface area and the MnO_2 molar volume impeded the measurement of the proton diffusion coefficients of the partially discharged MnO_2. Either $s\sqrt{D}$ [10] or BET surface area were used to estimate the proton diffusion coefficient. In my recent publication [11], the proton diffusion coefficient was measured by taking into consideration of the true electrochemically accessible surface area at various stages of the discharge of EMD electrode by means of AC impedance technique and the fitting based on the transmission line model. The electrochemically accessible surface area was determined by the change of the double-layer capacitance of the porous EMD electrode. A unique electrochemical test cells was designed to record the electrode expansion in situ during the discharge of the electrode, thus the change of the molar volume can be estimated from the change of the electrode volume.

Even though, the semi-infinite diffusion model was used for the fitting of the AC impedance results, Qu [11] noted that interpreting the results by the semi-infinite diffusion model for the proton diffusion inside the lattice of MnO_2 was questionable, since the condition for the semi-infinite diffusion model may not be met. EMD is well known as a highly disordered material with De Wolff (intergrowth of ramsdellite and pyrolusite) and microtwinning disorders. The crystallite size of commercially available EMDs are in the range from 20 to 200 Å, depending on how it is calculated. The proton diffusion at the practically useful potential (>0.45 V versus Hg/HgO) was believed only involving the [1 × 2] channels in the ramsdellite domains of the solid-state solution. Either De Wolff disorders or microtwinning, or other kinds of strains can interrupt the homogeneity of the ramsdellite unit and thus put obstacles along the proton diffusion pathway in the [1 × 2] channel. So a proton may travel across the whole distance of the diffusion length, especially at the late stage of the discharge, thus, the finite diffusion model may be more appropriate for the investigation of the proton diffusion inside the lattice of MnO_2 structure. To the best of my knowledge, it is the first report of combining AC impedance, transmission line model and finite diffusion model for the study of the proton diffusion inside EMD structure.

2. Experimental

2.1. Material

EMD was obtained from Kerr-McGee Corporation. KS6 synthetic graphite was from Lonza (now Timcal). Teflon suspension (T-30) used was from Dupont.

2.2. Electrolyte, and reference—and counter electrodes

An amount of 30 wt.% aqueous potassium hydroxide solution was used as the electrolyte in all experiments at 298 ± 1 K. All potentials reported were referred to Hg/HgO reference electrode immersed in KOH of the same concentration as the experimental electrolyte. A Ni mesh counter electrolyte was used.

2.3. Construction of EMD electrode and electrochemical cell

The detailed descriptions for the electrode construction and the electrochemical cell were reported previously [11]. The MnO_2 electrode was made with EMD and KS6 graphite at 9:1 weight ratio, 0.5 wt.% Teflon (dry material) was used as binder. Two grams of the mix was pressed to form a tablet with 22.0 ± 0.2 mm in diameter and 1.8 ± 0.2 mm in thickness. Two-compartment cell was used. The EMD working electrode and the counter electrode were housed in the separate cell compartments, which were linked by an electrolyte bridge. Spring pressure was applied to make sure good contact between the working electrode tablet and the Ni current collector. Hg/HgO reference electrode was connected to the working electrode compartment by Luggin capillary.

2.4. Experimental techniques and instrumental details

The AC impedance measurements were conducted by means of a Solartron Electrochemical Interface 1278 and Solartron Frequency Response Analysizer 1285 controlled by ZPLOT and CORRWARE software. ZVIEW was used for the fitting of the AC impedance data. The X-ray powder diffraction pattern of the EMD was collected using Simens D5000 powder diffractometer equipped with a Cu target X-ray tube and monochrometer. WIN-Crysize software from Simens (Now Brauker AXS) was used for the calculation of the crystallite size based on Warren–Averbach theory.

The EMD electrode was discharged under 30.8 mA g^{-1} (*C*/10 rate). The discharge was stopped at various stages of the depth of discharge (DOD). The electrode was put on rest until the potential variation between the cathode and the Hg/HgO reference electrode became less than ±5 mV/h. The AC impedance measurements were then carried out at OCV and ±10 mV potential amplitude.

3. Results and discussion

3.1. Theory and equivalent circuits

A porous MnO_2 electrode is constructed with MnO_2 and graphite particles of various size distributions. Packing of those particles results of pores with different sizes throughout the porous electrode. Pores with different size distributions have different time constants, and the ionic diffusion rate inside the pores of different sizes varies. In parallel to the proton diffusion throughout the lattice of MnO_2, the ionic diffusion is inside the matrix of the porous MnO_2 electrode. The complication of the ionic diffusion inside the porous electrode results from the fact that the ionic diffusion rate varies in the pores of different sizes. So the surface area of

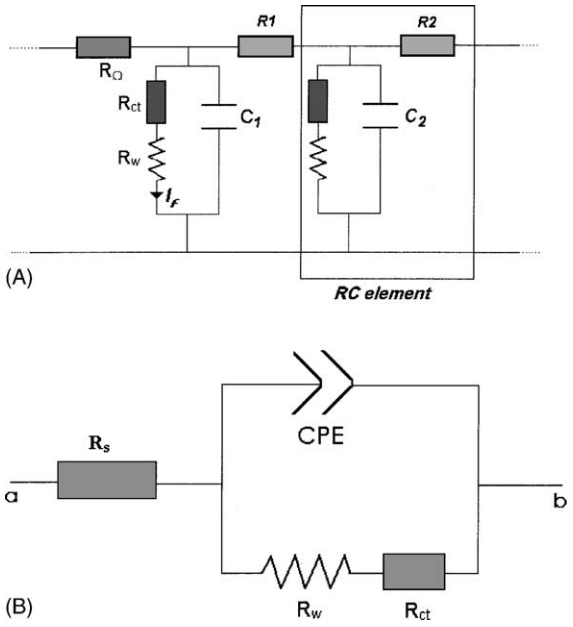

Fig. 1. (A and B) Transmission line equivalent circuit model used in the AC impedance fitting. R_s and R_Ω: Ohmic resistances; R_{ct}: Faraday resistance; C: distributed double layer capacitance; R: distributed resistance; R_w Warburg resistance; CPE: constant phase element.

the porous electrode, which can be accessed electrochemically, depends on the density of the discharge current. A good example to demonstrate the impact of porosity is the approximately inverse correlation between BET surface area of EMD and their discharge capacity in alkaline electrolyte [12]. Also, problems of different kind arise due to finite resistance of the particles and the supporting electrolyte, and to inter-particle contact resistance. The detailed discussion regarding the ionic diffusion in the matrix of a porous electrode can be found in the early publications [11,13,14].

A transmission line equivalent circuit was developed by De Levie [14] to represent the porous electrode involving Faraday charge transfer. The equivalent circuit was modified and applied to the study of porous MnO_2 electrode [11]. Fig. 1 shows the transmission line equivalent circuit. The detailed descriptions for the model can be found in the reference [11]. R_{ct} and R_w represent the charge transfer resistance and Warburg impedance for the reduction of MnO_2, respectively. C_{dl} is the double layer capacitance. The energy dissipation in the porous electrode can be represented by the distributed double layer capacitance and resistance in the RC transmission line. The mathematical equation of the RC transmission line has the same form as the diffusion equation. So the transmission line equivalent circuit in Fig. 1A can be simplified as in Fig. 1B. CPE is a constant phase element (CPE) and its impedance can be represented as [17].

$$Z = \sigma'\omega\left[\cos\left(\frac{1}{2}m\pi\right) - \mathrm{i}\sin\left(\frac{1}{2}m\pi\right)\right] \quad (1)$$

where σ is termed as the CPE factor and m is the CPE exponent.

A Warburg impedance represents the diffusion of charge carriers through a medium. The frequency of the modulation signal, alternatively the discharge current density, determines the depth of the charge carriers can travel. Lower frequency or lower discharge current density corresponds to the diffusion deeper into the material; higher frequency or higher discharge current density corresponds to the diffusion less deep into the material. If the medium is not thick enough, the charge carriers will penetrate the entire thickness during the low frequency modulation or the low current density discharge, thus finite Warburg impedance has to be used. On the other hand, if the thickness of the medium is large enough, the charge carriers cannot travel the entire length of the diffusion path even at the low modulation frequency or the low discharge current density ($\omega \gg D/\delta^2$, where ω is the modulation frequency, D is the diffusion coefficient of the charge carriers and δ is the diffusion length), then the impedance would be semi-infinite Warburg impedance. In the porous MnO_2 electrode, the interface of EMD particles is between their solid surface with the electrolyte in the pores, since the pore size is similar with or even smaller than the particle size of EMD, so even the average particle size of MnO_2 is less than 50 μm, for each individual EMD particles, they can be treated as a flat electrode instead of a spherical electrode. With the assumption that the proton diffusion inside MnO_2 is the rate determine step, Fick's second law can be written as

$$\frac{\partial C(l,t)}{\partial t} = D\frac{\partial^2 C(l,t)}{\partial^2 l} \quad (2)$$

The initial condition is

$$C(l,t)_{t=0} = C_0 \quad (3)$$

where C_0 is the initial proton concentration, it should be the initial proton concentration in the [1 × 2] channel or in the ramsedellite domain of EMD.

The first boundary condition is

$$\left(\frac{\partial C(l,t)}{\partial l}\right)_{l=0} = 0 \quad (4)$$

For the AC impedance measurement, another boundary condition is

$$\left(\frac{\partial C(l,t)}{\partial l}\right)_{l=d} = \frac{i_m \sin\omega t}{nsFD}$$

where i_m is the response current to the modulation potential and ω is the frequency of the AC signal.

In the case of the semi-infinite diffusion model, $\omega \gg D/\delta^2$, the Warburg impedance can be obtained by solving the diffusion Eq. (2) and expressed as [15]

$$Z_\omega = \sigma(1-\mathrm{i})\omega^{-1/2} \quad (6)$$

where

$$\sigma = \frac{V_m}{nFA(2D)^{1/2}}\frac{\partial V_{ocv}}{\partial x} \quad (7)$$

Then

$$D = \frac{1}{2}\left[\frac{V_m}{nFA\sigma}\frac{\partial V_{ocv}}{\partial x}\right]^2 \quad (8)$$

$\partial V_{ocv}/\partial x$ is the slope of the open circuit voltage (V_{ocv}) versus the mole fraction of MnO_2 and V_m is the molar volume of MnO_2. A is the electrochemically accessible surface area. All the parameters can be obtained experimentally [11].

In the case of the finite diffusion assumption, $\omega \ll D/\delta^2$, the complex graph (Nyquist plot) is a vertical line perpendicular to the real axis, and

$$D = \frac{\delta^2}{3R_l C_l} \quad (9)$$

where

$$C_l = \frac{d(-I_m)}{d(\omega^{-1})} \quad (10)$$

I_m is the imaginary impedance. R_l and C_l can be obtained from the Nyquist plot [16]. The true finite diffusion model obviously does not suit the case of the proton diffusion inside the lattice of EMD.

In the transition region between the semi-infinite and the true finite diffusion control, where $\omega \approx D/\delta^2$, the Nernst diffusion layer thickness, δ was comparable to the distance traveled by the diffusion species in the low frequency oscillating perturbations, then the impedance is given [17] as

$$Z_\omega = (1 - i)\sigma\omega^{-1/2}\tanh\left[\delta\left(\frac{i\omega}{D}\right)^{1/2}\right] \quad (11)$$

When

$$K = \sqrt{\frac{2\delta^2}{D}} \quad (12)$$

Then

$$Z'_\omega\,(\text{real}) = \frac{\sigma}{\sqrt{\omega}}\frac{(\sinh K\sqrt{\omega} + \sin K\sqrt{\omega})}{(\cosh K\sqrt{\omega} + \cos K\sqrt{\omega})} \quad (13)$$

$$Z''_\omega\,(\text{imaginary}) = \frac{\sigma}{\sqrt{\omega}}\frac{(\sinh K\sqrt{\omega} - \sin K\sqrt{\omega})}{(\cosh K\sqrt{\omega} + \cos K\sqrt{\omega})} \quad (14)$$

Both σ and K can be obtained by means of the least square fitting of the AC impedance results.

3.2. Fitting the AC impedance results based on the finite diffusion model

The AC impedance measurements for the EMD electrode were taken at various depths of the constant current discharge. Fig. 2 shows the discharge curve at 30.8 mA g^{-1} (C/10). The arrows indicate the time, at which the AC impedance measurements were taken. Fig. 3A and B shows the complex plane plots for the EMD electrode before discharge and at 50% DOD. The fitting results based on both the semi-infinite and the finite diffusion models are plotted with the experimental results for the comparison. It is obvious that the finite diffusion model fitted the experimental data better, especially in the low frequency range and for the partially discharged electrode. The fitting results for the non-discharged and the 50% DOD discharged EMD electrode based on the finite diffusion model are listed in Table 1. In order to obtain the diffusion coefficient from the finite diffusion model (Eq. (12)), the length of proton diffusion path (δ) has to be estimated.

3.3. Proton diffusion path and the estimation for its length

EMD is well known as a highly disordered material. In general, MnO_2 displays one of far the most complex

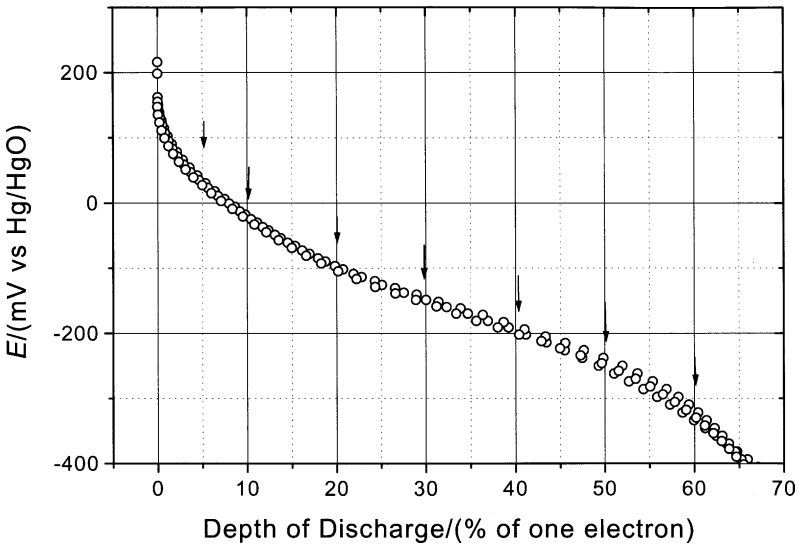

Fig. 2. Discharge curve for the constant current (30 mA g^{-1}) discharge of EMD electrode. Arrows indicate the DOD where AC impedance measurements were taken.

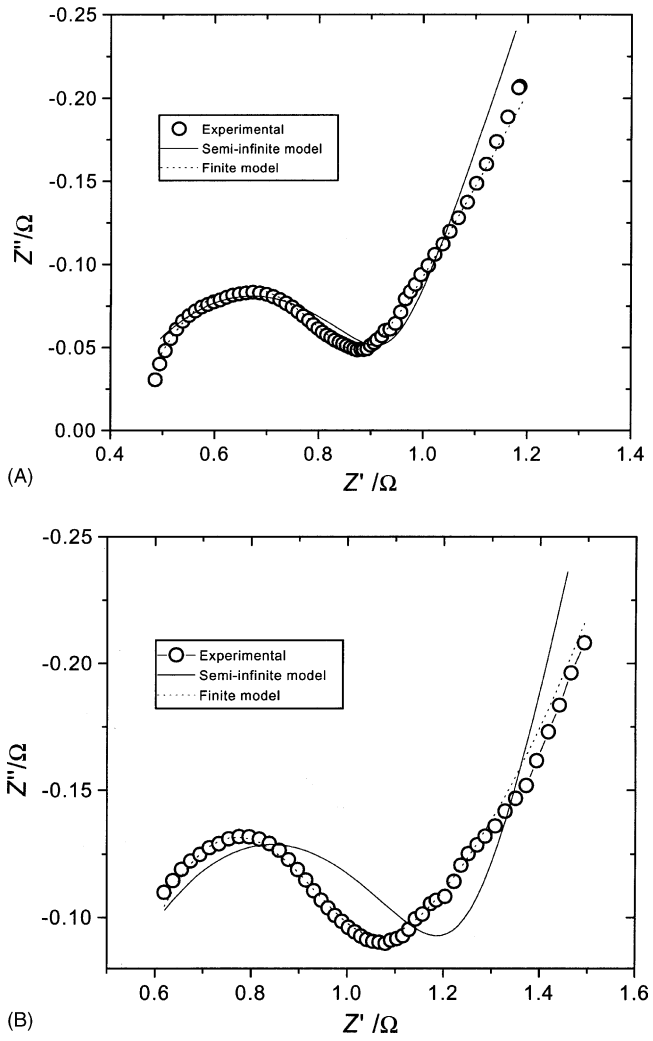

Fig. 3. AC impedance response for a non-discharged (A) and 50% DOD discharged EMD electrode (B). Numerical fitting were based on semi-infinite model (solid line) and finite model (dashed line).

series structure among the hcp $^{VI}MX_e$ compounds. The structure of MnO_2 of all kinds can be described as a distribution of cations Mn^{4+} in the interstices of a more or less close-packed network of oxygen atoms. The complexity of the MnO_2 structure results from the fact that several cation ordering schemes are possible. After studying the X-ray diffraction (XRD) patterns of the γ-MnO_2 samples, De Wolff [18] suggested that the crystal structure of γ-MnO_2 could be described as random intergrowth of pyrolusite layers in a ramsdellite matrix. Ramsdellite domains are closely related to pyrolusite structure, except that the single chains of edge-sharing octahedral are now replaced by double chains. The defect created by the intergrowth of pyrolusite chains does not affect the unit cell dimensions along *a*- and *c*-directions, but shorten the *b* dimension of ramsdellite unit cell. As the consequence of the introduction of pyrolusite domains into ramsdellite matrix, two kinds of tunnels co-exist in the γ-MnO_2 structure. They are [1 × 1] tunnels in the pyrolusite domains and [1 × 2] tunnels in the ramsdellite domains. De Wolf disorder model has been further proved and well adopted as the fundamental structure of γ-MnO_2. Despite all the success of De Wolff model, not all the features of X-ray diffraction of γ-MnO_2 can be account for by just using De Wolff disorder, for example, the frequent coalescence of lines h21 and h40, which are not modified by the layer disorder. Chabre and Pannetier [6] introduced another kind of defect identified as microtwinning, which occurs on the (0 2 1) and (0 6 1) growth planes of EMD. Microtwinning in ramsdellite has no effect on the anionic lattice, but results of a change in the Mn^{4+} distribution in the octahedral sites constructed by oxygen atoms. The immediate octahedral coordinated environment of manganese atoms is not changed.

In the light of the structural studies for γ-MnO_2, it has been long believed that within the range of the practically useful potential for the reduction of EMD, protons intercalate and diffuse mainly along [1 × 2] tunnels in the ramsdellite domains. The assumption was supported with the first principle calculation done by Cedar and co-workers [19]. In the lattice of γ-MnO_2, protons hop between localized oxygen sites and reside for most of the time at minimum energy sites, but eventually jump from on site to another overcoming the intersite energy barrier by a thermally activated process. The protons will travel along the path with minimum energy barrier. Cedar and co-workers estimated that the activation energy barrier for the proton diffusion in the pyrolusite domains along the [1 × 1] tunnel was 575 meV versus 200–400 meV for the proton diffusion in ramsdellite along the [1 × 2] tunnel.

The proton has 140 meV higher energy near the planar oxygen site than that near the pyramidal site; thus, protons diffuse along the [1 × 2] tunnel by hopping between the pyramidal oxygen ions on the opposite sides, the activation energy for each hopping was estimated 200 meV [19]. Therefore, the length for the proton diffusion should be the ramsdellite crystallite size. Fig. 4 shows the X-ray diffraction of the Kerr-McGee EMD. Typical five broad peaks of EMD were fitted by the least squares refinement method according to Lorentzian distribution. Each peak was indexed accordingly. The detailed index and positions of the peaks are listed in Table 2. The peaks, which are not affected by De Wolff disorder, are listed in *italics* in the table. The structure of ramsdellite is believed to be orthorhombic. Table 3 tabulates the parameters for the orthorhombic unit

Table 1
Fitting results for non-discharged and 50% DOD discharged EMD based on equivalent circuit in Fig. 1

Parameters	Non-discharged	50% DOD
Ohmic resistance, R_s (Ω)	0.448	0.476
Charge transfer resistance, R_{ct} (Ω)	0.508	0.447
CPE factor, σ'	14.7	36.7
CPE exponent, m	0.46	0.57
K' ($\sqrt{\delta^2/D}$) (s)	19.2	26.9

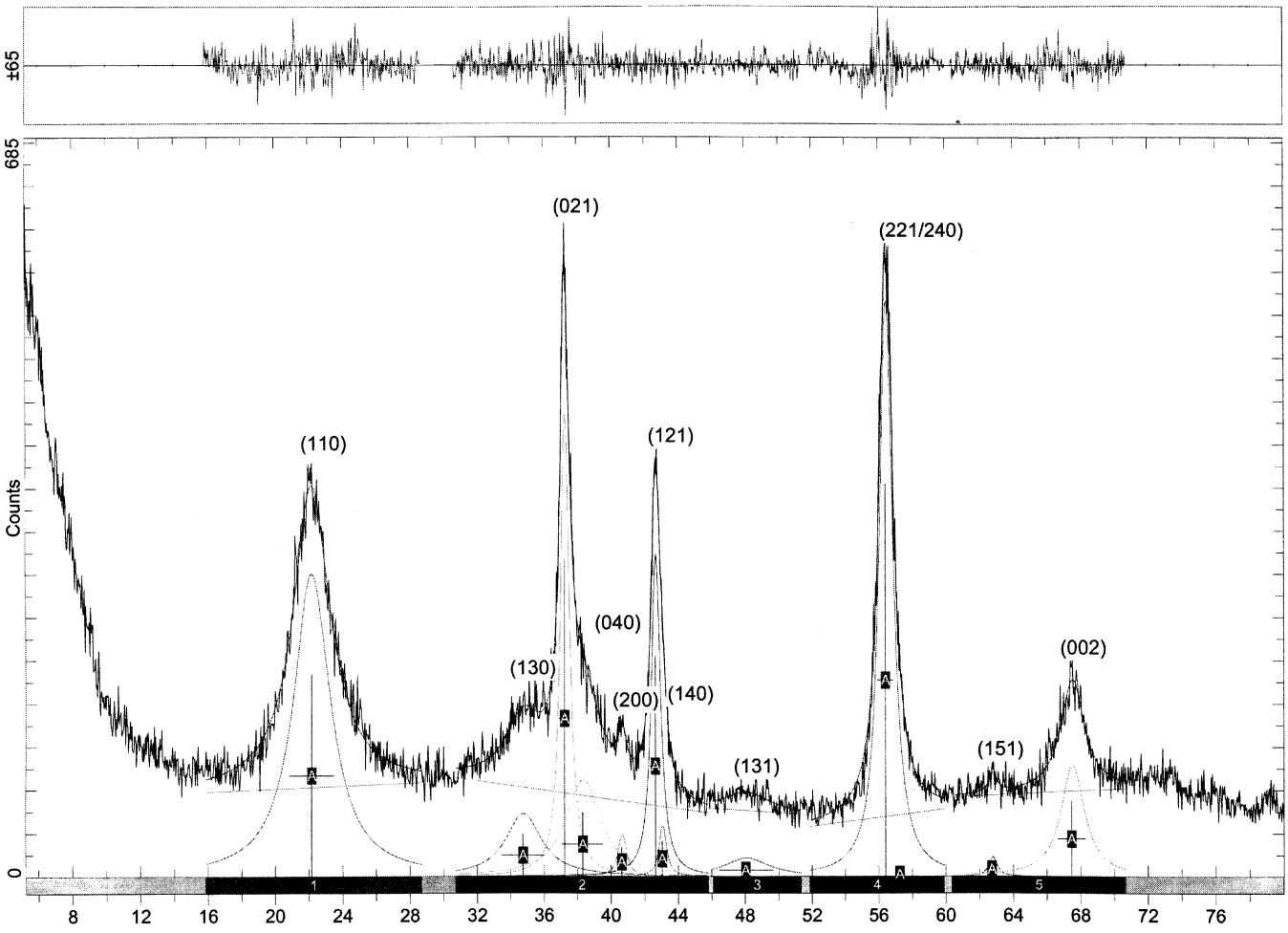

Fig. 4. XRD profile of the EMD. Lorentizian profile refinement results are plotted with experimental results. Peaks from the refinement are indexed.

cell calculated using only the peaks without being affected by De Wolff disorder.

It is the common practice among EMD and alkaline battery manufactures to calculate the crystallite size of EMD from (1 1 0) peak by means of Scherrer equation [20]:

$$\text{crystalsize} = \frac{K\lambda}{(\text{FWHM}^2 - S^2)\cos(\theta)} \quad (15)$$

where λ is the wavelength of the X-ray being used, FWHM stands for full width at half maximum, S is the instrumental line broadening and θ is the center position of the peak. In the case of EMD, the (1 1 0) X-ray diffraction peak is so wide that the instrumental broadening (S) can be ignored. The crystallite size calculated from the (1 1 0) peak through Scherrer equation is listed in Table 4. Even though Scherrer equation is well adopted to estimate the "effective" crystallite size of EMD, the results are questionable. As discussed previously, EMD is a highly defective material with various kinds of defects. There are three factors, which can broaden a diffraction peak and affect peak profile shape: crystallite

Table 2
Line positions of the EMD XRD patterns shown in Fig. 4

($h\,k\,l$)	2θ	
	Observed	Calculated
1 1 0	22.162	22.039
1 3 0	34.707	34.706
0 2 1	*37.241*	*36.567*
1 1 1 (0 4 0)	38.344	38.508
2 0 0	*40.619*	*40.523*
1 2 1	*41.475*	*41.995*
1 4 0	*42.684*	*43.085*
1 3 1	48.839	47.338
2 2 1	*56.420*	*55.420*
2 4 0	*57.272*	*56.603*
1 5 1	62.736	62.098
0 0 2	*67.456*	*65.017*

Peaks which are not affected by De Wolff disorder are listed in *italics*.

Table 3
The orthorhombic unit cell parameters for the EMD

Parameters	Angstrom (Å)
a	4.4487
b	9.5156
c	2.8666

Table 4
Crystallite size estimated from (1 1 0), (1 2 1) and (0 2 1) diffraction peak by two different theories

	(1 1 0)	(1 2 1)	(0 2 1)
Scherrer equation (Å)	22.1	110	95.8
Warren–Averbach (nm)	–	12.5	11.7

size, microstrain, which results from the internal stress, and could be associated with localized defects and instrument. Referring to Table 2, both De Wolff and microtwinning defects contribute to the (1 1 0) diffraction line broadening. So without taking into account microstrain, it may result of significant lower crystallite size by using Scherrer equation on (1 1 0) diffraction peak.

Another method is proposed in this paper to estimate the crystallite size of EMD based on Warren–Averbach theory [21] by taking into consideration both microstrain and instrumental contributions. The instrumental broadening can be corrected by using lanthanum hexaboride (LaB_6) single crystal (Standard Reference Material 660a from National Institute of Standard and Technology), this standard reference material (SRM) is made for use as a standard for calibration of diffraction line positions and line shapes determined through powder diffractometry. In order to estimate the crystallite size of ramsdellite, the diffraction peaks which were not affected by De Wolff disorder (those in *italics* in Table 2) were chosen for the calculation. Evidentially, (0 2 1) and (1 2 1) peaks are sharper than (1 1 0) peak. Besides instrumental broadening, peak broadening due to microstrain has to be corrected too, in order to obtain the crystallite size. Warren–Averbach theory involves the analysis of the peak profile shape, from which contribution due to crystallite size and microstrain are separated; Microstrain in materials increases the line width as a function of 2θ. The width from crystallite size and lattice distortion can be deconvoluted by Fourier transforming the peak profiles of the standard and unknown and plotting the Fourier coefficients as function of the ($h\,k\,l$) values of the measured reflections, a crystallite size distribution and a microstrain distribution are obtained, which yield an average crystallite size and root mean squared microstrain. Full utilization of Warren–Averbach theory involves the measurement of the complete profile of multiple orders of the same reflection, e.g. (1 1 0), (2 0 0), (3 0 0). Since it leaks the same reflection peaks in the XRD of EMD, additional assumptions were made, in which the crystallite size broadening has Lorentzian (Cauchy) profile and the microstrain broadening has a Gaussian profile. The detailed mathematics can be found in Warren's book [21]. Eqs. (16)–(19) summarize the method. The distribution of diffracted powder $P'_{2\theta}$ per unit length on a Dubye–Scherrer cone can be expressed as a Fourier series:

$$P'_{2\theta} = K(\theta)N\sum_{1}^{\infty}(A_n\cos(2pnh_3) + B_n\sin(2pnh_3)) \qquad (16)$$

The sin term in Eq. (16) can be ignored, since only such effects that broaden a peak profile symmetrically are assumed to be present:

$$A_n = A_n^{\text{size}} A_n^{\text{strain}} \qquad (17)$$

Assuming Lorentizian profile for size broadening and Gaussian curve for microstrain broadening,

$$A_n = F(\text{Lorentizian})\,F(\text{Gaussian}) \qquad (18)$$

where F stands for Fourier transform. Then

$$\ln A_n = \text{In}(e^{-x_1 n}e^{-x_2 n^2}) = -X_1 n - X_2 n^2 \qquad (19)$$

The coefficients X_1 and X_2 of the second-degree polynomial contain the information on crystallite size and microstrain.

Applying Warren–Averbach theory to the (1 2 1) and (0 2 1) diffraction peaks, the crystallite size for EMD can be calculated. The results are listed in Table 4 together with the crystallite size calculated based on Scherrer equation which, indeed resulted smaller crystallite size in all cases.

3.4. Proton diffusion coefficient in EMD

With the information of the crystallite size for the ramsdellite domain, which has been believed as the proton diffusion length, the proton diffusion coefficient can be then calculated from the fitting results of the AC impedance based on the finite diffusion model (Eq. (12)). The diffusion coefficients for the EMD at various stages of the discharge were estimated based on the crystallite size calculated from (1 1 0) peak by Scherrer equation, (1 2 1) and (0 2 1) diffraction peaks by Warren–Averbach theory. Fig. 5A and B shows the proton diffusion coefficients at various DOD estimated by the semi-infinite diffusion model and the finite diffusion model with the crystallite size estimated from (1 1 0) peak by Scherrer equation, respectively. Fig. 6 shows the comparison of the diffusion coefficients at various DOD with the crystallite size calculated by Warren–Averbach theory from (1 2 1) and (0 2 1) diffraction peaks. By comparing the results in Figs. 5 and 6, the diffusion coefficients obtained from the semi-infinite model and the finite diffusion model have the similar profile and within the range of 10^{-15} to 10^{16}.

It is worth to recognizing that, even though the crystallite size of non-discharged EMD was used as the length of proton diffusion path throughout the discharge at various stages, the actual length of the diffusion is unlikely to remain unchanged. The crystallite size of ramsdellite should remain unchanged until massive John–Teller distortion collapses the initial crystal structure of EMD. In this study, the crystallite size can be considered unchanged throughout the whole range of the discharge. However, the proton diffusion length may also relate to the proton concentration in the [1 × 2] tunnel. The H concentration increases as the discharge proceeds. This may explain why the finite diffusion model fitted the experimental results much better than

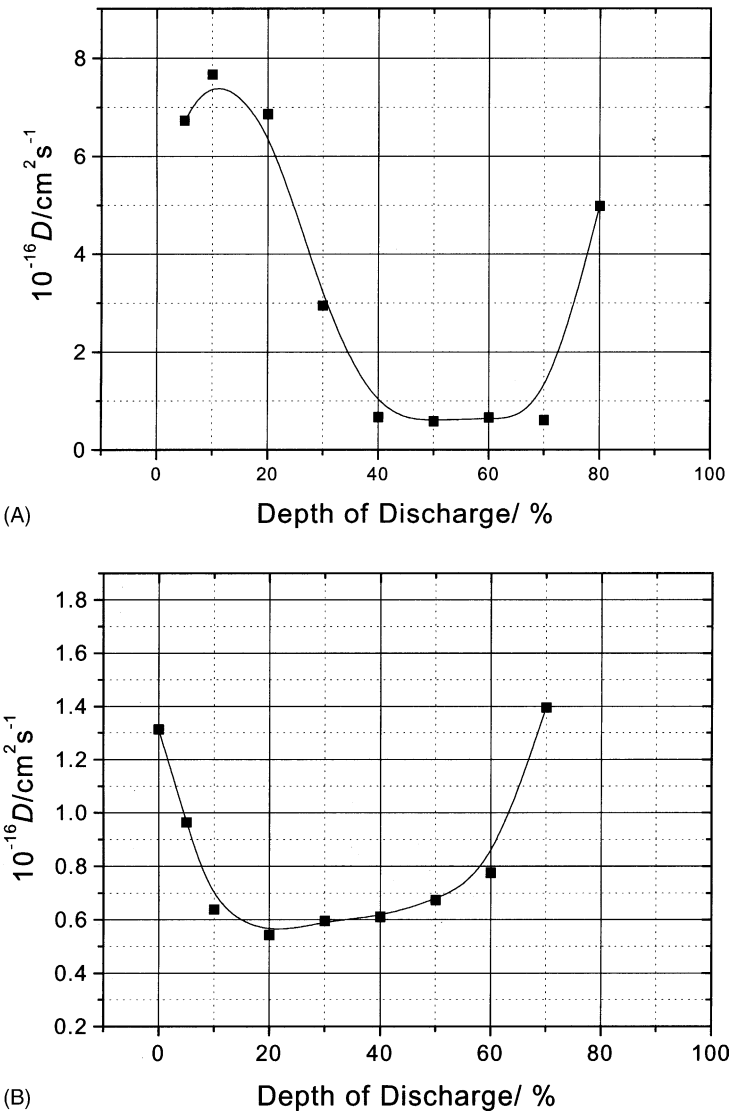

Fig. 5. Proton diffusion coefficients inside EMD at various depths of the discharge based (A) semi-infinite diffusion model and (B) infinite diffusion model with diffusion length calculated from (1 1 0) peak with Scherrer equation.

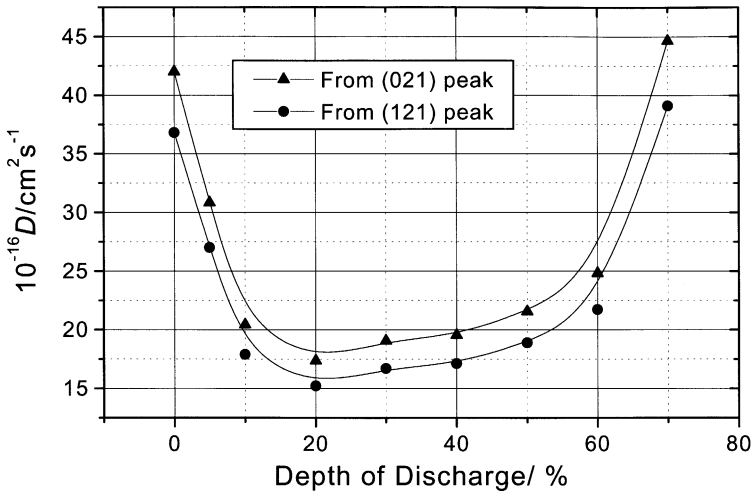

Fig. 6. Comparison of the proton diffusion coefficients inside EMD at various depths of discharge with Warren–Averbach method from (0 2 1) an (1 2 1) diffraction peaks, respectively.

the semi-infinite diffusion model for the partially discharged electrode.

4. Conclusions

The proton diffusion coefficients at various stages of the discharge have been estimated by means of AC impedance and numerical fitting techniques with finite diffusion model. The following points are of value to be noted:

1. Determination of proton diffusion coefficients inside the lattice of EMD is the essential step to the understanding of the proton intercalation process.
2. Combining with numerical fitting techniques, AC impedance is one of effective method to estimate the diffusion coefficients in solid state.
3. Three factors can contribute to the XRD peak broadening. They are instrument, crystallite size and microstrain.
4. EMD is a highly disordered material, (1 2 1) and (0 2 1) diffraction line, which are not affected by De Wolff disorder are better choices than (1 1 0) diffraction line for the calculation of the crystallite size of EMD.
5. Warren–Averbach method, which takes into consideration all three factors, yields more realistic results for the estimation of the crystallite size of EMD than Scherrer equation, which did not take into account of microstrain.
6. The finite diffusion model fitted experimental results better than the semi-infinite diffusion model.
7. Proton diffusion in EMD occurs in the $[1\times2]$ tunnel of the ramsdellite domains. The crystallite size of ramsdellite can be treated as the proton diffusion length.

References

[1] A. Kozawa, J.F. Yeager, J. Electrochem. Soc. 115 (1968) 1003.
[2] A. Kozawa, R.A. Powers, J. Electrochem. Soc. 113 (1966) 870.
[3] A. Kozawa, R.A. Powers, Electrochem. Tech. 5 (1967) 535.
[4] A. Kozawa, R.A. Powers, J. Electrochm. Soc. 115 (1960) 112.
[5] S. Atlung, T. Jacobsen, Electrochim. Acta 21 (1976) 575.
[6] Y. Chabre, J. Pannetier, Prog. Solid State Chem. 23 (1995) 1.
[7] J.J. Coleman, Trans. Electrochem. Soc. 90 (1946) 545.
[8] A.B. Scott, J. Electrochem. Soc. 107 (1960) 941.
[9] F. Kornfeil, J. Electrochem. Soc. 109 (1962) 349.
[10] J.P. Gabano, J. Seguret, J.F. Laurent, J. Electrochem. Soc. 117 (1970) 147.
[11] D.Y. Qu, Electrochim. Acta 48 (2003) 1675.
[12] T.N. Andersen, J.M. Derby, Electrochemistry in Transition, Plenum Press, New York, 1992, p. 655.
[13] D.Y. Qu, H. Shi, J. Power Sources 74 (1998) 99.
[14] R. De Levie, Electrochim. Acta 8 (1963) 751.
[15] C. Ho, I.D. Rastrick, R.A. Huggins, J. Electrochem. Soc. 127 (1980) 343.
[16] X.X. Yuan, N. Xu, Univ. Chem. 12 (2002) 27.
[17] L. Dawson, D.G. John, J. Electroanal. Chem. 110 (1980) 37.
[18] P.M. De Wolff, Acta Crystallogr. 12 (1959) 341.
[19] D. Balachandran, D. Morgan, G. Cedar, J. Solid State Chem. 166 (2002) 91.
[20] D.A.J. Swinkels, R.P. Williams, Batteries Battery Mater. 15 (1996) 1.
[21] B.E. Warren, Progress in Metal Physics, vol. 8, Pergamon Press, London, 1959, p. 147.